IMPROVED INFRASOUND EVENT LOCATION

Michael S. O'Brien[1], Douglas P. Drob[2], and J. Roger Bowman[1]

Science Applications International Corporation[1] and Naval Research Laboratory[2]

Sponsored by Army Space and Missile Defense Command

Contract No. W9113M-06-C-0027

ABSTRACT

The purpose of this project is to improve the ability to locate infrasound events by improving the Horizontal Wind Model (HWM) used in the prediction of infrasound observables, in particular, travel time and back azimuth. Our general approach uses new wind data to develop a higher-resolution and more accurate HWM and tests the performance of Ground to Space (G2S) specifications based on the new HWM, relative to those based on HWM-93 using a large set of ground-truth events. We assembled a preliminary data set of 180 events with which to exercise our statistical framework for testing the effect of atmospheric wind models on the accuracy of infrasound event locations. We also assembled wind data representing a 100-fold increase compared to those used for HWM-93 and incorporated these wind data into the mechanism used to generate improved HWMs. We applied this mechanism to construct a preliminary version of HWM-07, and demonstrated that this preliminary model displays some important features that were missing from HWM-93, such as wind velocities of up to 70 m/s at an altitude of 110 km. We created an efficient mechanism to trace rays through atmospheric models for a large suite of infrasound source-station pairs. Initially, we have based our generation of travel-time and back-azimuth predictions on the HARPA 3-D ray-tracing programs. We refined the statistical framework for testing the effect of atmospheric wind models on predictions and applied it to first arrivals for a preliminary data set of 251 source-receiver pairs from 108 events to evaluate and compare predictions made against the existing, baseline atmospheric specifications for our study, G2S and HWM-93/MSISE-00, on which it is based, above 50 km. As expected, we find that G2S more often and more accurately predicts stratospheric first arrival times and back azimuths, whereas the two models are both equally poor at predicting thermospheric arrival times and back azimuths. It is for thermospheric arrivals that we expect the most improvement to result from the improvements of HWM-07.

Report Documentation Page

Form Approved
OMB No. 0704-0188

1. REPORT DATE	2. REPORT TYPE	3. DATES COVERED
SEP 2007		**00-00-2007 to 00-00-2007**

4. TITLE AND SUBTITLE	5a. CONTRACT NUMBER
Improved Infrasound Event Location	5b. GRANT NUMBER
	5c. PROGRAM ELEMENT NUMBER
6. AUTHOR(S)	5d. PROJECT NUMBER
	5e. TASK NUMBER
	5f. WORK UNIT NUMBER
7. PERFORMING ORGANIZATION NAME(S) AND ADDRESS(ES) **Science Applications International Corporation,1710 SAIC Drive,McLean,VA,22102**	8. PERFORMING ORGANIZATION REPORT NUMBER
9. SPONSORING/MONITORING AGENCY NAME(S) AND ADDRESS(ES)	10. SPONSOR/MONITOR'S ACRONYM(S)
	11. SPONSOR/MONITOR'S REPORT NUMBER(S)

12. DISTRIBUTION/AVAILABILITY STATEMENT
Approved for public release; distribution unlimited

13. SUPPLEMENTARY NOTES
Proceedings of the 29th Monitoring Research Review: Ground-Based Nuclear Explosion Monitoring Technologies, 25-27 Sep 2007, Denver, CO sponsored by the National Nuclear Security Administration (NNSA) and the Air Force Research Laboratory (AFRL)

14. ABSTRACT
see report

15. SUBJECT TERMS

16. SECURITY CLASSIFICATION OF:			17. LIMITATION OF ABSTRACT	18. NUMBER OF PAGES	19a. NAME OF RESPONSIBLE PERSON
a. REPORT **unclassified**	b. ABSTRACT **unclassified**	c. THIS PAGE **unclassified**	**Same as Report (SAR)**	**10**	

OBJECTIVES

The primary purpose of this project is to improve our general ability to locate infrasound events by improving the HWM used in the prediction of infrasound observables. We do this using recent wind measurements and direct infrasound observations.

A second purpose of this project is to evaluate, statistically, the abilities of new and existing models to locate infrasound events and predict the principal infrasound observables, arrival time and back azimuth. We do this by comparing model predictions against a large set of infrasound observations.

RESEARCH ACCOMPLISHED

Background

The source location problem is a central element of nuclear explosion monitoring. In regional scenarios, it can provide important corroboration of explosive events but only if signals can be reliably attributed. Source location and, thus, location-related observables are central to source attribution. In remote regions that are not well monitored by other land-based technologies, such as the southern oceans, infrasound may provide the only information that constrains location.

The reliability of infrasound source locations depends on the reliability with which signal features can be predicted from source properties. This requires detailed knowledge of sound propagation in the atmosphere and the physical properties that control it, in particular, the static sound speed and wind field. The state of the art in representing the atmospheric properties pertinent to infrasound propagation is the Naval Research Laboratory (NRL) G2S model (Drob and Picone, 2000; Drob et al., 2003). This model combines climatological data captured in MSISE-00 and HWM-93 with numerical weather prediction (NWP) data, such as the Navy Operational Global Atmospheric Prediction System (NOGAPS) and the National Oceanic and Atmospheric Administration (NOAA) National Center for Environmental Prediction Global Forecast System (NCEP-GFS). Wind models that are based solely on climatology often substantially underestimate tropospheric and stratospheric wind jets, which leads to significant under prediction of the fraction of energy that is ducted through these layers (Drob and Picone, 2000; Drob et al., 2003). The utilization of the near-real-time NWP data in G2S significantly improves estimates of tropospheric and stratospheric wind jets that profoundly influence sound speed at lower altitudes (<50 km).

While the G2S models are the most comprehensive atmospheric representation available, significant infrasound residuals for thermospheric arrivals are still obtained using them. Le Pichon et al. (2005) found that back-azimuth residuals using G2S models averaged several degrees for repeated thermospheric propagation paths. Others (e.g., O'Brien and Shields, 2004) observe that, where only thermospheric arrivals are predicted, the predicted times systematically over-predict observed arrival times. The principal source of these discrepancies appears to be the wind model in the mesospheric/lower thermospheric (MLT) region, where weather data cannot assist. Recent direct measurements of winds at higher elevations indicate that HWM-93 significantly underestimates winds there. Stronger MLT winds imply larger azimuthal deflections, lower turning heights, and shorter travel times for predicted arrivals.

HWM-07 Prototype

The purpose of this task at this stage of the project is to demonstrate that we can successfully incorporate all the new atmospheric wind data into the mechanism to be used to generate HWMs. A new, unified HWM empirical model framework, applicable to *all* altitude regions and allowing for greater extensibility (e.g., future increases in resolution) has been developed and is in intermediate testing phases. The revamped HWM horizontal formulation now includes a complete linear and orthogonal spatiotemporal spectral basis set:

$$\begin{aligned} U(\tau,\lambda,\delta,\theta) = &\sum_{s=0}^{S}\sum_{l=0}^{L}\sum_{n=l}^{N} C^{r}_{s,l,n}\Psi_1(\tau,\delta,\theta) - C^{i}_{s,l,n}\Psi_2(\tau,\delta,\theta) + B^{r}_{s,l,n}\Psi_3(\tau,\delta,\theta) + B^{i}_{s,l,n}\Psi_4(\tau,\delta,\theta) \\ &+ \sum_{s=0}^{S}\sum_{m=0}^{M}\sum_{n=l}^{N} C^{r}_{s,m,n}\Psi_1(\tau,\lambda,\theta) - C^{i}_{s,m,n}\Psi_2(\tau,\lambda,\theta) + B^{r}_{s,m,n}\Psi_3(\tau,\lambda,\theta) + B^{i}_{s,m,n}\Psi_4(\tau,\lambda,\theta) \end{aligned} \quad (1)$$

In this equation $U(\tau,\lambda,\delta,\theta)$ represents the zonal wind field at a given model level as a function of day of the year, longitude, local solar time, and latitude, respectively. The vector spherical harmonics (VSH) are expressed in the complex spectral amplitudes coefficients, $C_{r,i},B_{r,i}$. A similar relationship for $V(\tau,\lambda,\delta,\theta)$ exists given the basis function parity/orthogonality relationship U: $\{C_r,C_i,B_r,B_i\}$ and V: $\{B_r,B_i,-C_r,-C_i\}$. The Fourier time modulated VSH basis functions are

$$\Psi_1^{s,m,n}(\theta,\lambda,\tau) = \frac{-1}{\sqrt{n(n+1)}}\frac{dP_n^m(\theta)}{d\theta}[\cos(m\lambda)\cos(s\tau)+\cos(m\lambda)\sin(s\tau)] \quad (2)$$

$$\Psi_2^{s,m,n}(\theta,\lambda,\tau) = \frac{1}{\sqrt{n(n+1)}}\frac{dP_n^m(\theta)}{d\theta}[\sin(m\lambda)\cos(s\tau)+\sin(m\lambda)\sin(s\tau)] \quad (3)$$

$$\Psi_3^{s,m,n}(\theta,\lambda,\tau) = \frac{-m}{\sqrt{n(n+1)}}\frac{P_n^m(\theta)}{\cos(\theta)}[\sin(m\lambda)\cos(s\tau)+\sin(m\lambda)\sin(s\tau)] \quad (4)$$

$$\Psi_4^{s,m,n}(\theta,\lambda,\tau) = \frac{-m}{\sqrt{n(n+1)}}\frac{P_n^m(\theta)}{\cos(\theta)}[\cos(m\lambda)\cos(s\tau)+\cos(m\lambda)\sin(s\tau)] \quad (5)$$

where $P_{n,m}(\theta)$ is the normalized associated Legendre polynomials and (s,l,m,n) are the seasonal, local time, longitudinal, and latitudinal spectral wave numbers, respectively. For maximum wave numbers of S = 2, L = 3, M = 2, and N = 8, there are 580 non-degenerate unknowns per model level.

The vertical variations in the HWM-07 model are represented by 5 km B-spline weighting kernels (e.g., De Boor, 1968), as illustrated in Figure 1. The HWM-07 empirical model specifications for the zonal and meridional wind components are thus given by the equation $[U,V] = \Sigma\alpha_i(z)U_i(\tau,\lambda,\delta,\theta)$, where $\alpha_i(z)$ is the amplitude of the respective weighting kernel in the altitude domain d_i.

The new model formulation and implementation also trivializes future increases in spectral resolution and input data set density for the foreseeable future. Linearization allows the replacement of the non-linear Levenberg-Marquard parameter estimation procedure with a straightforward linear least-squares estimation procedure (e.g., Rogers, 1996):

$$\hat{x} = x_a + (K^T S_\varepsilon^{-1} K + S_a^{-1})^{-1} K^T S_\varepsilon^{-1}(y - Kx_a) \quad (6)$$

$$\hat{S} = (K^T S_\varepsilon^{-1} K + S_a^{-1})^{-1} \ . \quad (7)$$

In this equation $\hat{x}$ is the model parameter estimates; x_a is an a priori estimate of the model spectral parameters [i.e., $\alpha(z)*C_r, C_i, B_r, B_i$], based on a previous iteration and data subset; variable K is the forward spectral matrix [i.e., the model basis functions $\Psi(\tau,\lambda,\delta,\theta)$]; S is the covariance matrix of the model parameter estimate; S_a is the covariance matrix of the a priori model parameter estimate; y is the observations; and S_ε is the covariance matrix or inverse uncertainty of the observations.

The data used to generate the new models are briefly summarized in O'Brien et al. (2006). The entire set of $O(10^9)$ data is far too large to be fit at once. Instead, we update the coefficients iteratively, at each step introducing a new random sub-sample of about 70,000 to 160,000 data from the entire set, depending on the altitude region. This limits working memory requirements to less than 10 GB yet allows all data to eventually influence the model coefficients. With each

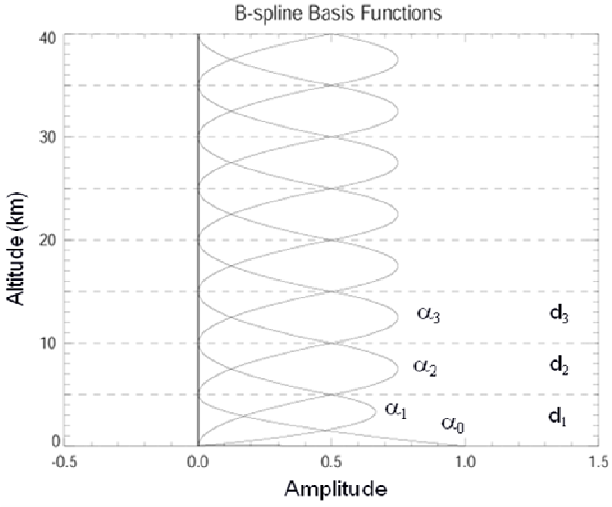

Figure 1. Example of B-spline weighting kernels.

iteration, the coefficient variances decrease; that is, the coefficients improve, so that their influence in the next iteration increases over that of the next data sub-sample. Iteration continues until the coefficients converge. The number of data sampled from each data set/type and altitude region is made roughly equal in each iteration. Data sets that span sparse regions, or are the only data set in a given domain, are weighted higher. Conversely, data sets that overlap with many other data sets are weighted lower.

Codes for the new model formulation, including a new client module that will be distributed to users when the model coefficients are more mature, are more compact, succinct, understandable, efficient, and extensible than the legacy HWM-93 code. The new client module also supports OpenMP parallelization of key subroutines and do loops, allowing for exploitation of recent advances in low-cost, multi-core processor architectures and supporting FORTRAN compilers. This will be important further into this project when large ensembles of infrasound propagation calculations for ground-truth events are required to refine and tune model parameters and performance.

Preliminary Model Comparisons—HWM-07 versus HWM-93

Although HWM-07 can be regarded as only preliminary at present, it already shows markedly improved agreement with the newer data over HWM-93. As anticipated, the preliminary HWM-07 has much higher amplitude tidal winds in the 85 to 135 km altitude regions, in part because the representation of the diurnal migrating tide is now in line with more-recent measurements and scientific understanding. It also includes the observed seasonal variations, phase quadratures, and hemispheric symmetries and asymmetries of the respective zonal and meridional wind components. Typical improvements are illustrated in the top and bottom rows of Figure 2, which shows WINDII wind measurements (Shepherd et al., 1993) averaged in overlapping 2-hour bins and 10 degree latitude bins (black lines), together with corresponding point-for-point averages from HWM-93 (blue lines) and the current preliminary HWM-07 (red lines). The top row illustrates the strong zonal winds observed on either side of the meridional wind maxima that are better captured in HWM-07 but are almost absent in HWM-93. At higher latitudes, some winds now captured exceed 70 m/s. However, there are fitting issues still to be resolved in HWM-07. The bottom row of plots illustrates the strong meridional winds observed at subtropical latitudes (±22.5º). These are clearly captured better by HWM-07 than by HWM-93, but not fully, thus motivating further model adjustments.

In addition, HWM-07 contains fewer features believed to be artifacts than does HWM-93. For example, the amplitude of semidiurnal tidal oscillations, in particular the zonal component near the equator above 115 km, is significantly weaker in HWM-07 than in HWM-93, as illustrated in Figure 3. HWM-07 much better matches the WINDII satellite data in the left panel, which show no evidence of the strong diurnal component.

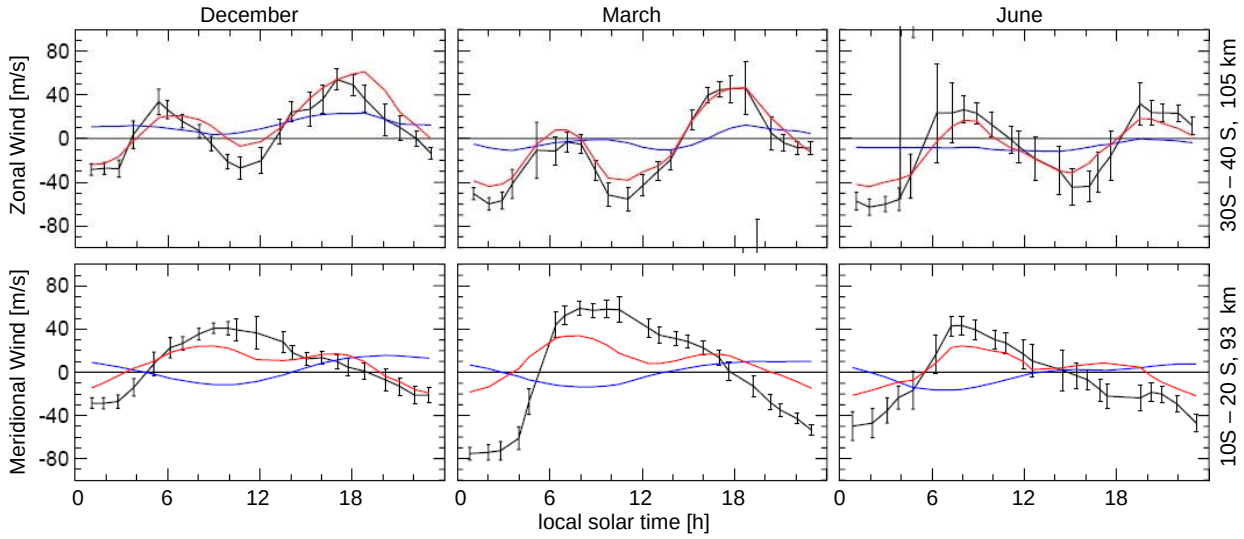

Figure 2. Examples of WINDI wind data (Shepherd et al., 1993—black lines) averaged in one-hour time-of-day bins showing significantly improved predictions of HWM-07 (red lines) over HWM-93 (blue lines). Top: HWM-07 captures most of zonal winds averaged between 30S and 40S at an altitude of 105 km, while HWM-93 captures little. Bottom: HWM-07 captures more of the meridional winds between 10S and 20S than HWM-93, but further improvement is still possible.

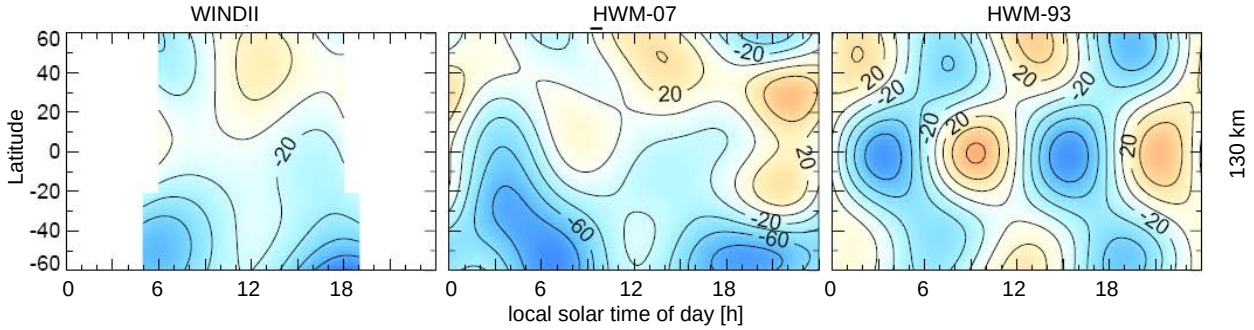

Figure 3. Comparison of December zonal winds [m/s] at 130 km altitude from WINDI wind data (Shepherd et al., 1993) with predictions of HWM-93 and HWM-07. Spurious tidal harmonic artifacts that are present in HWM-93 are eliminated in HWM-07.

Most importantly, more accurate wind specifications of greater magnitude in the 95 to 120 km altitude region will result in significantly lower thermospheric ducting heights for infrasound. This will lead to shorter predicted travel times and less molecular attenuation. Travel time calculations utilizing current HWM-93 specification generally over predict thermosphere wave guide travel times (e.g., O'Brien and Shields, 2004). For example, arrival times predicted by ray tracing though G2S for four of the five observed arrivals from the Watusi chemical test explosion on September 9, 2002, are over predicted by 200 to 700 seconds; the first ray predicted to land along the source-receiver azimuth of the fifth station does so about 60 km past the station. All of these rays are predicted to turn at heights of 105 to 140 km. In addition, given the current frequency-dependent infrasonic attenuation coefficients (e.g., Sutherland and Bass, 2005), current PE and ray-tracing calculations of many ground-truth events where thermosphere arrivals are observed predict too much attenuation. For the case of significant cross-track lower thermosphere wind conditions, the new wind specifications will result in the calculation of greater azimuthal deviations, again in line with infrasonic observations (e.g., Le Pichon et al., 2006).

Statistical Assessment Method

The virtues and shortcomings of any wind model must be evaluated with respect to the accuracy with which it predicts infrasound data. In this respect, the most reliable observables are arrival time and back azimuth. O'Brien et al. (2006) developed statistics for quantifying the overall abilities of models to predict these for an arbitrary set of source-receiver combinations. In particular, statistics comparing predictions from two models *p* and *q* have the form

$$F_{p-q} = \frac{\chi_p^2 / N_p}{\chi_q^2 / N_q} \sim F_{N_p, N_q}, \tag{8}$$

where χ_k^2 is a sum of squares of the N_k residuals from model *k*; F_{p-q} can be built from any subset of observations, such as travel times or back azimuths. Later, we compute $F_{\text{HWM-G2S}}$ for HWM93-MSISE00 and G2S using only travel times, only back azimuths, and both. If, as we believe, G2S better predicts the observations, *F* will be greater than 1. Our assertion is that F_{pq} is approximately distributed as F_{N_p, N_q}, against which we can test its statistical significance. This depends on having good estimates for the residual uncertainties. We estimate these for fractional travel time *T* and back azimuth deviation from the receiver-source azimuth *A* using the following error models:

$$\sigma_T^2 \approx \frac{\sigma_t^2}{T^2} + \frac{\sigma_r^2}{R^2} + \frac{\sigma_e^2}{R^2} + \frac{\sigma_\tau^2}{T^2} + \frac{\sigma_{MT}^2}{T^2} \tag{9}$$

$$\sigma_A^2 \approx \sigma_a^2 + \frac{\sigma_r^2}{R^2} \qquad \sigma_{MA}^2 \tag{10}$$

Here, σ_t, and σ_a are uncertainties in observed arrival time and back azimuth; σ_r, σ_e, and σ_t are the uncertainties in source time, location, and elevation. These are one of the subjects of the next section. The actual uncertainties introduced into A and T by the model are σ_{MT} and σ_{MA}, which we seek to quantify. We assume that uncertainty in station location is relatively insignificant.

Preliminary Infrasound Event Data Set

The meaningfulness of assessment statistics grows with the number of observations that can be compared to model-based predictions. Thus, a significant component of this project is devoted to collection and analysis of ground truth event data. In principle, any event is usable within our framework, as long we can reasonably estimate σ_r, σ_e, and σ_t, which strongly influence σ_A and σ_T and, hence, the statistical power of each datum and its weight in the assessment statistics. Without accurate uncertainties, we risk polluting statistics with erroneous data whose value is erroneously overestimated. Thus, a significant component of the ground-truth analysis is devoted to estimating the source parameter uncertainties. Typically, the less well we can estimate the source parameters themselves, the less well we can estimate their uncertainties, so we conservatively eliminate poorly constrained events, such as large earthquakes and rocket launches, having spatially and temporally extensive sources. Other events with large estimated uncertainties may be eliminated subsequently if they appear to degrade the statistics disproportionately.

The map in Figure 4 shows source-receiver paths for the 180 events for which we have estimated σ_r, σ_e, and σ_τ to be small enough to admit either travel time or back azimuth to the observation set. Of these, 108 are in western North America and 31 at the Zheleznogorsk mining site in Russia. The remaining events are distributed fairly randomly around the globe.

In the last year we have improved the ground-truth data for over 120 events. Source parameters for all the events are stored in the Monitoring Research Program infrasound database found on the web at http://www.rdss.info.

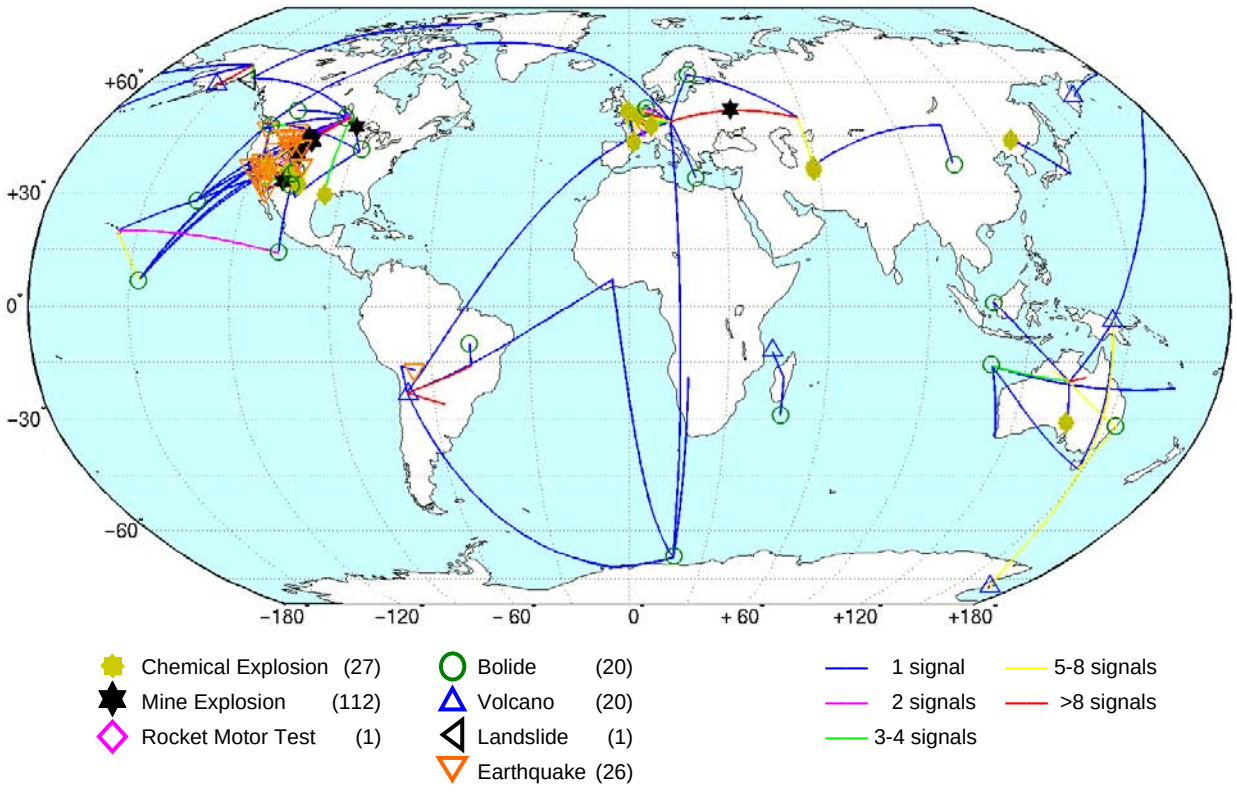

Figure 4. Map of events in the preliminary infrasound event data set.

Atmospheric Propagation Modeling

We have obtained model-based predictions by tracing rays through the candidate models using the HARPA 3-D ray-tracing programs packaged with InfraMAP (Norris and Gibson, 2006). We have not attempted here to account for terrain except by elevating the sources and receivers to their actual heights above sea level. Future computations will account for terrain using the NRL RAMPE ray tracer and the terrain-correcting versions of HARPA recently released in beta with InfraMAP.

We executed eigenray searches for 108 events for which we have already generated G2S models, including 640 arrivals from 251 source-receiver pairs. Even for this fraction of the anticipated final data set and only two atmospheric models, G2S and HWM93-MSISE00, the ray tracing represents a large computational task – it required about 160 hours of CPU time on an AMD Opteron 285 microprocessor, although instabilities with finding the intersections between rays and the ground may account for a significant portion of that time. The task also demands significant bookkeeping, since the ray-tracing programs must be executed separately for each source-receiver-model scenario, each producing multiple outputs. To facilitate the repeated task of computing eigenrays for an arbitrarily large set of source-station pairs, we have created efficient UNIX scripts for running the HARPA programs, extracting the prediction data from its outputs, and assimilating its results into an Oracle database, where the evaluation statistics are computed.

However, the process of mapping predictions to arrivals is more difficult to automate or even objectify. In some way this must be done by correlating the values of measured and predicted observables, such as arrival time, back azimuth, slowness, amplitude, and duration. Even some unobservable predicted ray properties such as turning height or number of ground reflections may influence the mapping. It is not always clear how much weight each predicted and observed datum should get in the process, creating a significant combinatorial problem, especially if there are multiple observed and predicted arrivals for a given source-receiver pair.

Ultimately, we will have to face these vagaries, but here we present statistical comparisons based on a more illustrative mapping that avoids them altogether. We map only first arrivals, each to the predicted arrival with the best fitting arrival time. The mapping does not guarantee or even purport to be the best mapping in the sense of all the observables—some mappings are certain to be incorrect—but it is unambiguous. We also consider separate statistics for arrivals predicted to have maximum turning heights in the troposphere/stratosphere (TS) region (<65 km) and the MLT region (> 65 km) because we expect predictions based on G2S to differ significantly from those based on HWM93-MSISE00 only where the rays spend most of their time at TS altitudes. Figure 5 (a) illustrates that, in fact, all the predicted turning height are easily separated into these height regions, all having maximum turning heights below 55 km (TS) or above 100 km (MLT).

As expected, using G2S leads to predictions of significantly more TS arrivals (about 1/3 more) and more arrivals overall than HWM93-MSISE00. This is illustrated in the Figure 5(b) histogram of the percentage of source-receiver pairs for which the models predicted any arrival, grouped by the ducting region predicted for the first arrival. The anticipated superiority of G2S is confirmed in Table 1, in which we have tabulated $F_{\mathrm{G2S/HWM}}$ and the corresponding significance levels for all combinations of travel-time and back-azimuth data in each of the TS and MLT ducting regions. From all perspectives G2S has outperformed HWM93-MSISE00 ($F_{\mathrm{G2S/HWM}} > 1$), mostly with high statistical significance. The histograms of travel-time residuals in Figure 6 illustrate that a major reason for the domination is the replacement of a number of highly erroneous MLT first-arrival predictions of HWM93-MSISE00 by much more accurate TS predictions of G2S. This leads to dramatically better predictions in both ducting regions, especially of travel times.

Table 1. $F_{\mathrm{G2S\text{-}HWM}}$ statistics for first arrival prediction residuals and associated significance levels in parentheses. Values greater than 1 indicate that G2S residuals are smaller.

Data Type	Maximum Turning Height		
	< 65 km	> 65 km	All
Travel times only	1.84 (99.7%)	1.20 (82.9%)	1.40 (98.9%)
Back azimuths only	1.13 (67.5%)	2.11 (99.9%)	1.66 (100%)
Travel time and back azimuths	1.34 (95.7%)	1.84 (100%)	1.70 (100%)

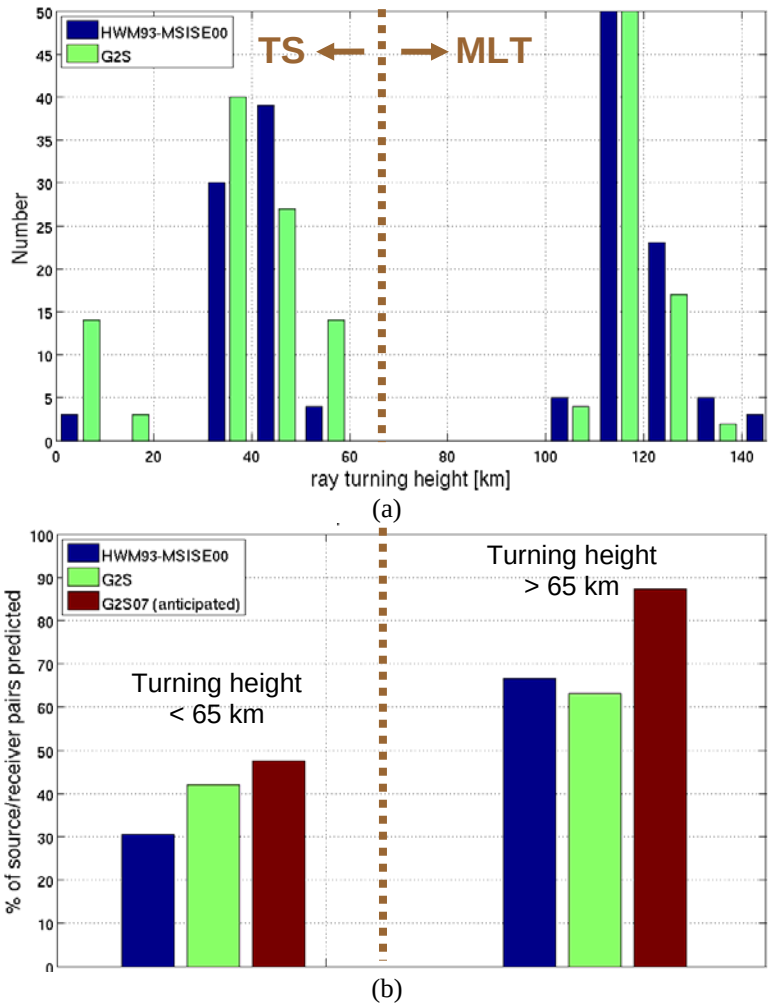

Figure 5. (a) Turning heights of predicted first -arrival predictions from G2S and HWM93-MSISE00 define well-separated troposphere/stratosphere (TS) and mesosphere/lower thermosphere (MLT) turning height domains. (b) Percentages of source-receiver pairs predicted by each model grouped by the turning heights of the predicted first arrivals. G2S predicts significantly more lower-atmospheric arrivals. We anticipate a similar increase in the number of predicted MLT arrivals from HWM-07.

We anticipate that HWM07-MSISE00 and G2S-07 will provide additional improvement to MLT predictions over their existing counterparts. Figure 6(b) shows the strong tendency of either HWM-93-based model to over predict travel times. Some of this is no doubt the result of failure to predict much faster TS arrivals. However, some is the simple result of over predicting the MLT travel times. With generally stronger MLT winds, HWM-07 will have higher overall effective sound speeds in the MLT region. This will have a two-fold effect to shorten MLT travel times by increasing the propagation speed and lowering predicted MLT turning heights, thereby shortening propagation paths. A less likely improvement is that increased mesospheric winds will effectively raise the top stratospheric duct in some cases, thereby increasing the number of faster stratospheric predictions.

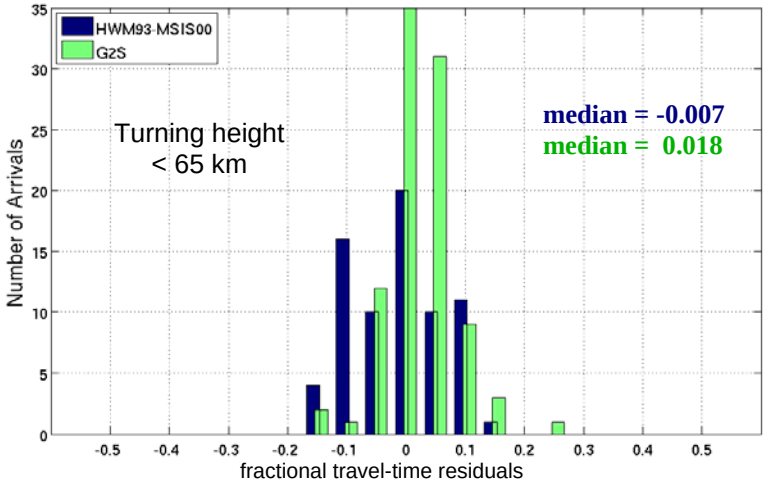

(a)

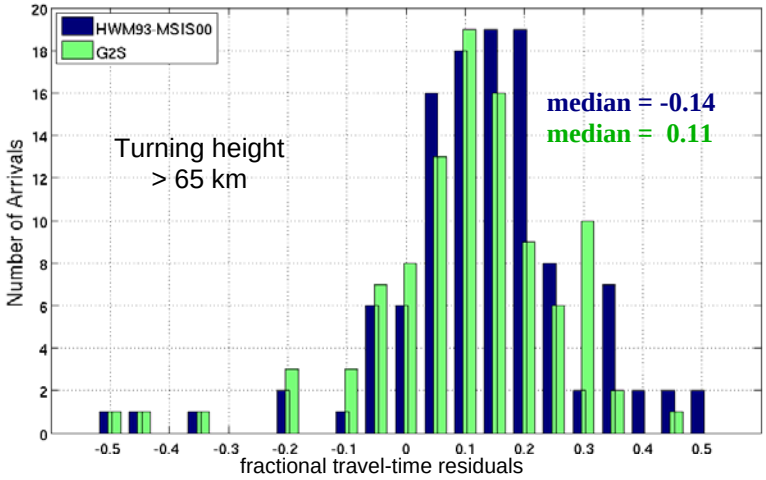

(b)

Figure 6. Fractional travel-time residuals for first arrivals predicted to turn at heights within (a) the TS region below 65 km and (b) the MLT region above 65 km. Travel times in both regions are better predicted by G2S. MLT residuals are strongly biased toward late prediction, which HWM-07 is intended to address.

CONCLUSIONS AND RECOMMENDATIONS

We have begun construction of the new atmospheric wind specification HWM-07. The new model is structurally and computationally superior to its predecessor HWM-93. Already, we have achieved significantly improved fit to many wind data sets gathered since HWM-93 was created and reduced model artifacts. Continued refinement of the model parameters is still required to fit all the salient features that are manifest in the wind data.

We have refined our data set of ground-truth events, carefully assessing source parameters and their accuracy. We have increased the number of constraining events to almost 200 and will continue to expand this set. We have developed statistical and computational machinery required to generate arrival predictions by ray tracing for a large set of source-receiver pairs to test against the observations. We have applied the machinery to first arrivals from HWM93-MSISE00 and G2S, clearly and quantitatively demonstrating the anecdotally accepted prediction superiority of G2S arrivals.

REFERENCES

De Boor, C. (1968). On uniform approximation by splines, *J. Approx. Theory* 1: 219–235.

Drob, D. P., J. M. Picone, and M. Garces (2003). Global morphology of infrasound propagation, *J. Geophys. Res*. 108 (D21): 4680, doi: 10.1029/2002JD003307.

Drob, D. P. and J. M. Picone (2000). Statistical performance measures of the HWM-93 and MSISE-90 empirical atmospheric models and the relation to infrasonic CTBT monitoring, in *Proceedings of the 22nd DoD/DOE Seismic Research Symposium: Planning for Verification of and Compliance with the Comprehensive Nuclear-Test-Ban Treaty (CTBT)*, Vol. 1, pp. 161–169.

Le Pichon, A., E. Blanc, D. P. Drob, S. Lambotte, J. X. Dessa, M. Lardy, P. Bani, and S. Vergniolle (2005). Infrasound monitoring of volcanoes to probe high-altitude winds, *J. Geophys. Res*. 110, D13106, doi: 10.1029/2004JD005587.

Le Pichon, A., K. Antier, and D. Drob (2006), Multi-year validation of the NRL-G2S wind fields using infrasound from Yasur, *InfraMatics* 16: 1–9.

Norris, D. and R. Gibson (2006). User's guide for InfraMAP (Infrasonic Modeling of Atmospheric Propagation): Version 5.1, BBN technical memorandum W2078, July.

O'Brien, M. and G. Shields (2004). Infrasound source locations using time-varying atmospheric models, in *Proceedings of the 26th Seismic Research Review: Trends in Nuclear Explosion Monitoring*, LA-UR-04-5801, Vol. 2, pp. 660-669.

O'Brien, M., J. Bowman, and D. Drob (2006). Improved infrasound locations through refining atmospheric models using wind data and ground-truth infrasound events, in *Proceedings of the 28th Annual Seismic Research Review: Ground-Based Nuclear Explosion Monitoring Technologies*, LA-UR-06-5471, Vol. 2, pp. 926-935.

Rogers C. D. (1996). *Inverse Methods for Atmospheric Sounding*. Singapore: World Scientific Pub. Co.

Shepherd, G. G., G. Thuillier, W. A. Gault, B. H. Solheim, C. Hersom, J. M. Alunni, J.-F. Brun, S. Brune, P. Charlot, D.-L. Desaulniers, W. F. J. Evans, F. Girod, D. Harvie, R. H. Hum, D. J. W. Kendall, E. J. Llewellyn, R. P. Lowe, J. Ohrt, F. Pasternak, O. Peillet, I. Powell, Y. Rochon, W. E. Ward, R. H. Wiens, and J. Wimperis (1993). WINDII—The wind imaging interferometer for the upper atmosphere research satellite, *J. Geophys. Res.* 98: 725–10, 750.

Sutherland, L. C. and H. E. Bass (2005). Atmospheric absorption in the atmosphere up to 160 km, *J. Acoust. Soc. Am*. 115: 1012–1032, doi: 10.1121/1.1631937.